RSC Advances

ROYAL SOCIETY OF CHEMISTRY

www.rsc.org/advances

Sorption of arsenate onto magnetic iron-manganese (Fe-Mn) biochar composites

Shengsen Wang[1], Bin Gao[1]*, Yuncong Li[2], Yongshan Wan[2], Anne Elise Creamer[1]

1. *Department of Agricultural and Biological Engineering, University of Florida, Gainesville, FL 32611*
2. *Tropical Research and Education Center, Soil and Water Science Department, University of Florida, Homestead, FL 33031*

* Corresponding author: phone: (1) 352-392-1864 ext. 285, email: bg55@ufl.edu

Abstracts

Bimetal adsorbents attract much attention because of their good sorption ability to arsenate (As(V)). In this work, biochar-supported bimetal adsorbents were prepared through either direct pyrolysis of Fe and Mn ions treated pinewood biomass (FMM) or co-precipitation of Fe and Mn ions onto pinewood biochar (FMB). The two Fe-Mn biochar composites were characterized using X-ray diffraction (XRD), X-ray photoelectron spectroscopy (XPS), scanning electron microscopy (SEM), and energy-dispersive X-ray (EDS) analyses. Characterization results suggest that maghemite (γ-Fe_2O_3) and manganosite (MnO) are dominant metal crystals in FMM, while manganese ferrite (MnFe2O4) is the dominant bimetal crystal in FMB. Batch sorption experiments showed that maximal As(V) sorption of FMB and FMM were 3.44 and 0.50 g kg^{-1} respectively, which were higher than that of the unmodified biochar. As(V) sorption by FMM and FMB decreased with increasing solution pH (between 3-9). Results of this work suggest that co-precipitation is more effective in preparing magnetic Fe-Mn biochar composites for As(V) removal.

Keywords: biochar; manganese ferrite; bimetal oxides; arsenate; magnetic adsorbents

1. Introduction

Arsenic (As) originating from naturally-occurring and anthropogenic sources is detrimental to human health and environmental safety [1]. Arsenate (As(V) and As(III) are two dominant inorganic As forms in natural environment. As contamination has been well documented in some Asian countries and northern American countries [2]. Long term consumption of As polluted water may cause cancer and other related diseases. Therefore, stringent regulations have been proposed by U.S. Environmental protection Agency (U.S.EPA), which prescribes the maximum allowance concentration is as low as 10 μg L^{-1} in drinking water [3]. Great efforts have been devoted to reclaim the As contaminated water. Because of its good removal efficacy and easiness of operation, the adsorption approach excels other treatment technologies for As, and attracts extensive search for high-efficient and cost-effective sorbents [4, 5].

Carbon (C) materials such as activated carbon, carbon nanomaterials, and biochar have also been utilized as adsorbents for various contaminants. However, these materials could not meet satisfactory needs, due to their low sorption ability for As. Compared to activated carbon and carbon nanomaterials, biochar is a less expensive C material that attracts attention as good sorbent for various organic and inorganic contaminants including some heavy metals. However, biochars usually have negative surface potential with low sorption ability to anions [6] including As. Thus, many attempts have been implemented to increase the As removal efficiency by modifying the pristine biochars. Because naturally-occurring and synthetic metal hydrous and anhydrous oxides, hydroxides, and oxyhydroxides, such as iron (Fe) oxide, manganese (Mn) oxide, and aluminum (Al) oxides, have been extensively studied as sorbent for As removal [7-10]. Biochars are therefore modified with colloidal and nano-sized oxyhydroxides of single metal,

such as Al [11], Fe [12], Mg [13], and Mn [5], and naturally occurring minerals [14], to improve their performance on As sorption.

Metal (M) ferrite (MFe_2O_4) has a cubic crystal structure, in which M and Fe occupy tetrahedral and octahedral cation sites, respectively [15, 16]. $MnFe_2O_4$ has attracted much attention because of its widespread use in catalysis [17] and Li-ion battery [18]. Recently, bimetal spinel nanocrystals, such as metal ferrites, have been found to have extraordinary performances in reclamation of environmental pollution, particularly with respect to the treatment of As [4, 19, 20]. For example, excellent As(V) and arsenate As(III) sorption abilities were observed by $MnFe_2O_4$ [4], copper ferrite [21], cobalt ferrite [4], and magnesium ferrite [20] in the literature.

Because of excellent sorption capacity for As, $MnFe_2O_4$ is thus proposed to modify pristine biochars to improve As removal efficiency. The resulting engineered biochars are usually in form of composites with $MnFe_2O_4$ being distributed and supported within the carbon matrix. Recently, $MnFe_2O_4$ has been combined with graphene oxides to form nanocomposites with enhanced sorption ability to As in aqueous solution [19]. However, nanosized or colloidal Mn ferrite and graphene oxides will complicate the operation and separation. Because of its abundance and relatively low cost, biochar would be a good supporting material for bimetal spinel nanocrystals. To the best of the authors' knowledge, none of the previous works have studied biochar-based bimetal spinel nanocrystals.

The overarching objective of this work was to develop novel bimetal biochar composites for the removal of As(V) from aqueous solution. Two types of magnetic Fe-Mn biochar adsorbents were prepared through either pyrolyzing pinewood biomass pretreated with Mn and Fe ions or co-precipitation of the two metal ions onto pinewood biochar. The adsorbents were tested for their As(V) sorption capacity in batch experiments. The specific objectives of this

work were to: (1) compare two modification methods in preparing magnetic Fe-Mn oxides biochar composites, (2) characterize the biochar composites, and (3) determine the sorption ability of the biochar composites to As(V) in aqueous solution.

2. Materials and Methods

2.1 Reagents

All chemicals of reagent grade were dissolved with deionized (DI) water (18.2 MΩ) (Nanopure water, Barnstead). Ferric chloride hexahydrate ($FeCl_3 \cdot 6H_2O$), manganese chloride tetrahydrate ($MnCl_2 \cdot 4H_2O$), granular sodium hydroxide (NaOH), concentrated hydrochloric acid (HCl), sodium arsenate dibasic heptahydrate ($Na_2HAsO_4 \cdot 7H_2O$), sodium nitrate ($NaNO_3$) were purchased from Fisher Scientific.

2.2 Biochar preparation

Loblolly pine (*Pinus taeda*) wood pretreated with Fe and Mn ions was used to prepare the Fe-Mn modified biochar (FMM) through pyrolysis. The biomass was oven dried overnight at 80^{o}C and then milled into < 2mm fragments with a mechanic miller. The ground biomass was passed both 1 and 0.425 mm size sieves, and size between 0.425 and 1 mm was collected for later use. 25 g feedstock was added to 100 mL of solution containing both 0.01 mol $MnCl_2 \cdot 4H_2O$ (2.0 g) and 0.02 mol $FeCl_3 \cdot 6H_2O$ (5.4g). The admixture was well mixed and suspended for 2 h at room temperature (22 ^{o}C) and oven dried at 80 ^{o}C overnight. The dried mixture was loaded into a tube furnace (MTI, Richmond, CA) and pyrolyzed for one hour in a constantly purged N_2 environment at a peak temperature of 600˚C. Previous studies have shown that, under this condition, $MnCl_2$ and $FeCl_3$ may be converted into their respective metal oxides [5, 12]. The unmodified pinewood derived biochar (PB) was also made as a control.

$MnFe_2O_4$ modified biochar (FMB) was synthesized following the co-precipitation procedures of Zhang et al [4]. Briefly, PB (5g) was added to 25 mL DI water, agitated with a magnetic stirrer, and continuously purged with N_2 gas for 30 min. 2.0g $MnCl_2 \cdot 4H_2O$ and 5.4g $FeCl_3 \cdot 6H_2O$ were then dissolved in biochar suspension, when N_2 gas were purged continuously, followed by drop-wise addition of 0.85 mL concentrated HCl. The suspension was completely transferred to 250 mL 1.5M NaOH preheated at 80 ^oC under continuous N_2 gas protection. The reaction was continued for 4 h at 80 ^oC. The resulting biochar composites was vacuum filtered through a 0.22 μm pore size nylon membrane filters (GE cellulose nylon membrane) and dried at 80 ^oC for 12 hours. The dried biochars were passed through 0.425 mm and 1mm sieves, the size 0.425-1 mm was washed several times with DI water, dried at 80 ^oC, and then saved in sealed contained for later use.

2.3 Biochar characterization

Total C, nitrogen (N) and hydrogen (H) contents in FMM and FMB were determined with a CHN Elemental analyzer (Carlo-Erba NA-1500). The FMM and FMB were prepared with AOAC method and total Fe and Mn contents were analyzed by an inductively coupled plasma-atomic emission spectrometry (ICP-AES, Perkin-Elmer Plasma 3200).

Brunauer-Emmett-Teller (BET) specific surface area was determined using a NOVA 1200 analyzer [22, 23]. Surface topography and elemental composition and distribution were obtained with scanning electron microscope (SEM) using a JEOL JSM-6400 Scanning Microscope, equipped with energy dispersive X-ray spectroscopy (EDS, Oxford Instruments Link ISIS).

Elemental composition of biochar surfaces and valence states of Mn, Fe and O were analyzed by an X-ray photoelectron spectroscopy (XPS) with a PHI 5100 series ESCA

spectrometer (Perkin-Elmer). An Al X-ray source was used with a 93.90 eV passing energy between binding energy between 0 and 1400 eV. High-energy resolution scans of O1s and Fe2p and peaks were obtained with passing energy of 23.50 eV at binding energy of 524–538 eV and 705-735eV, respectively.

Fe and Mn bearing crystals on biochar surface were identified using X-ray diffractometer (XRD) (Philips Electronic Instruments) equipped with a CuKα radiation source, and scans were carried out between diffraction angles 2-80^{o} with cavity mounting.

Thermal analysis of pristine biochar and FMM and FMB was performed using thermogravimetric analysis (TGA) with a Mettler Toledo's TGA/DSC1 analyzer, with combustion temperature between 25 and 700 ^{o}C under air atmosphere.

2.4 Adsorption kinetics and isotherm

Adsorption kinetics of As(V) onto biochar were determined following the procedure of Zhang et al. [12]. Briefly, about 0.05 g of biochar was added to 20 mL of 0.05 M $NaNO_3$ solution containing 20 mg L^{-1}As(V) solutions in each of digestion vessels (68 mL, Environmental Express) at room temperature (22 ± 0.5 ^{o}C). Thus, adsorbent concentration was about 2.5 g L^{-1} for all treatments. Previous studies have shown that this amount of $NaNO_3$ (ionic strength) has little/no effects on the rate of the adsorption of As(V) onto adsorbents such as metal and bimetal oxides [4, 24-27]. The pH of initial sorption solutions was adjusted with diluted HCl or NaOH to 7.5. The vessels with sorption mixtures were placed onto a rotary shaker and agitated at 40 rpm until sampling. At each sampling time (0, 0.5, 1, 2, 4, 8, 12, 24 and 48 h), three of the vessels were removed from the shaker and each suspensions was immediately filtered through 0.22 μm pore size nylon membrane filters (GE cellulose nylon membrane). The filtrate was collected to

determine As(V) concentration. The sorption of As(V) was calculated as difference of As(V) concentration in initial and final solutions.

Adsorption isotherms were determined in 0.05 M $NaNO_3$ solution at different As(V) concentrations. 20 mL As(V) (roughly 0-20 mg L^{-1}) solutions containing biochar were kept in 68 mL digestion vessels (Environmental Express). The pH of initial sorption solutions of different As concentrations was adjusted with diluted HCl or NaOH to 7.5. The suspension was agitated on a rotary shaker for 24 h. Final suspension was passed 0.22 μm pore size nylon membrane filters. As(V) adsorption was calculated as the difference of concentrations between initial solution and final solution.

As(V) sorption in both kinetic and isotherms studies were triplicated. The kinetics was fitted with first order, second order and Elovich mathematical models, and the isotherm data was fitted with Langmuir and Freundlich model. These models were described in detail in previous work [28].

2.5 Desorption studies

Biochar surface becomes negatively charged at high pH which facilitates desorption of negatively charged As oxyanions [29]. 0.1 M NaOH has satisfactory desorption efficiency for As(V)-loaded $MnFe_2O_4$ although a more concentrated NaOH shows better desorption capacity [4]. 0.1 M NaOH was also able to desorb chromium loaded biochars with good efficiency [30]. Thus, desorption studies were carried out in 0.1 M NaOH solution. To initiate desorption experiment, 0.10 g sorbents were incubated in 40 mL of 20 mg L^{-1} As(V) solution for 48 h, centrifuged, and then rinsed with DI water three times. The experiment was replicated three times The sorbent was then desorbed in 20 mL of 0.1 M NaOH for 48 h, and subsamples were collected at different time intervals to determine desorption progress with time.

2.6 As(V) sorption at different pH

pH casts influence on sorption in solution by affecting both surface charges of sorbents and speciation of As (V) oxyanions. pH effect on sorption is dependent on reaction mechanisms between sorbents and sorbates. Sorption curves of contaminants at different pH is usually obtained to predict the maximal sorption [4]. In this study, the effect of pH on As(V) sorption was determined at pH between 3 and 9. 20 mL of As(V) (40 mg L^{-1}) solutions were adjusted to designated pH with 0.1 M NaOH and HCl. The sorption with 0.05 g sorbents was conducted in 0.05 mM NaNO3 solutions and followed procedure described in *2.4*, and was terminated after 24 h. Sorption at each pH has been replicated three times.

2.7 Statistical analysis

TGA curves were made with Excel ® 2010 and Sigmaplot ® 12.0 software (Systat Software, Inc., San Jose, California, USA). The sorption kinetics and isotherms data was analyzed with SAS ® 9.4 (SAS Institute, Cary, NC) for standard deviation. The data was fitted with different mathematical models with SigmaPlot 12.0. As(V) speciation data as a function of pH was obtained by visual MINTEQ 3.1 (Jon Petter Gustafsson, KTH, Sweden) (I =0.05M, As(V)= 40mg L^{-1}) and plotted in the distribution diagram with SigmaPlot 12.0.

3. Results and Discussion

3.1 Physicochemical properties

C was the dominant element in both pristine PB and FMM (Table 1). The pyrolysis of Fe and Mn treated biomass (FMM) produced a composite with higher C content (75.1%) than biochar composites synthesized by direct precipitation of $MnFe_2O_4$ (FMB) (35.1%). The total C

content decreased slightly from 84.7% in PB to 75.1% in FMM, but drastically to 35.1% in FMB (Table 1). Total Mn contents in FMM and FMB were 54 and 95 times, and total Fe contents were 84 and 121 times higher than that in PB, respectively (Table 1). That is, the content of Fe and Mn in FMB was 1.76 and 1.44 times higher than that in FMM, respectively (Table 1). The atomic ratio of Mn and Fe was 0.54 in FMB based on the results of elemental analysis (Table 1). O content in FMB was about 4 times that in FMM and PB, indicating more metal oxides. This implies that more Mn and Fe oxides were impregnated in FMB than FMM during the fabrication process. As a result, both the FMM and FMB showed good magnetic properties (Figure S1, supporting information).

Table1. Elemental composition, surface area, and pore volume of PB, FMM and FMB.

	C	N	H	O	Mn	Fe	BET surface area	BJH Pore volume
	%, mass						$m^2\ g^{-1}$	$mL\ g^{-1}$
PB	84.7	0.61	2.3	12.26	0.05	0.08	360.2	0.007
FMM	75.1	0.47	1.9	13.44	2.76	6.33	386.7	0.019
FMB	35.1	0.38	1.7	48.84	4.85	9.13	280.0	0.175

Compared to the 'clean' carbon surfaces in PB (Figure S2d, supporting information), some particles were soldered on the carbonaceous surfaces in both FMM and FMB (Figure S2e and f, supporting information). The particles on the FMB surfaces were relatively smaller and denser than on FMM surfaces. EDS elemental analysis shows the atomic ratio of Mn and Fe was 0.58 (Figure S3, supporting information), close to 0.53 obtained from total elemental analysis (Table 1). EDS elemental mapping analysis shows that Mn and Fe distribution pattern matched

well in FMB (Figure 1 g and h), while there was a bigger discrepancy in FMM (Figure 1c and d). This indicates Fe and Mn oxides do not always reside on the same location of C surfaces in FMM, and independent metal oxides may have formed. In contrast, Fe and Mn in FMB appeared concurrently as a single crystal with atomic ratio close to 2, which implies that bimetal oxides formed within the biochar.

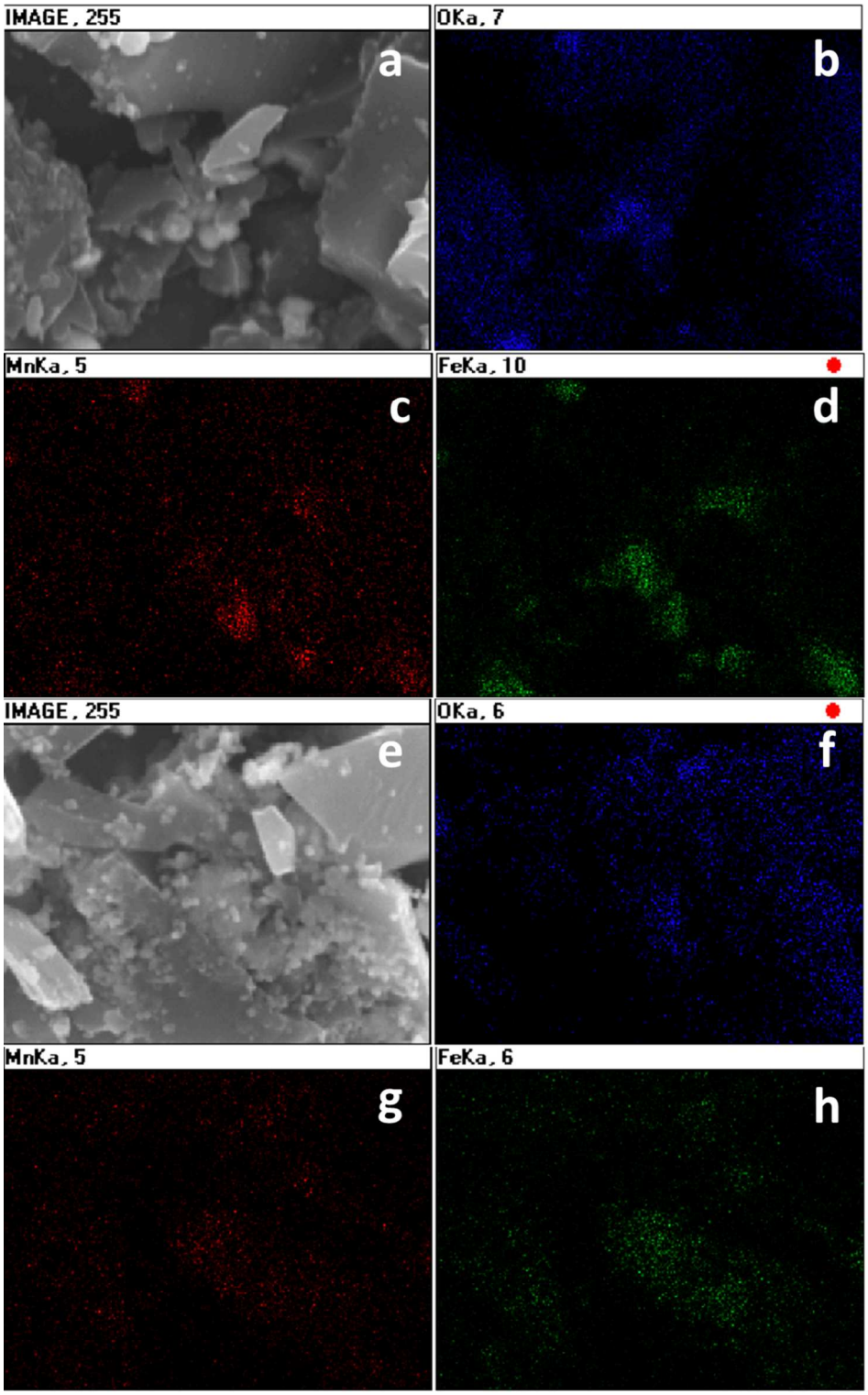

Figure 1. SEM/EDS elemental mapping analysis (10,000 x) for FMM (surface topography (a) and O (b), Mn (c), and Fe (d) distribution map), and FMB (surface topography (e) and O (f), Mn (g), and Fe (h) distribution map).

The crystallites on both FMM an FMB surfaces were ascertained with XRD analysis (Figure 2). FMB diffraction patterns showed that d-spacings were 4.903, 3.001, 2.558, 2.117, 1.638, and 1.502 Å (Figure 2), which match the diffraction patterns for jacobsite ($MnFe_2O_4$) [31]. XPS peaks showed binding energy for Fe2p1/2 and 3/2 are 724.7 and 711.3 eV, respectively (Figure S4b, supporting information), confirming the valance states of Fe in jacobsites. FMM had the diffraction d-spacing at 2.999, 2.530, 2.109, 1.624, and 1.486 Å (Figure 2a), which match either maghemite or magnetite. The XPS binding energy for Fe2p1/2 and 3/2 are 711.5 and 724.7 eV, respectively (Figure S4a, supporting information), corresponding to maghemite with trivalent Fe [14]. The peaks at d-spacing of 2.189, 1.543, 1.314, and 1.259 Å match manganosite (MnO) diffraction peaks [5]. Thus, the dominant crystals in FMM were both γ-Fe_2O_3 and MnO; while bimetal oxides, $MnFe_2O_4$ only formed in FMB.

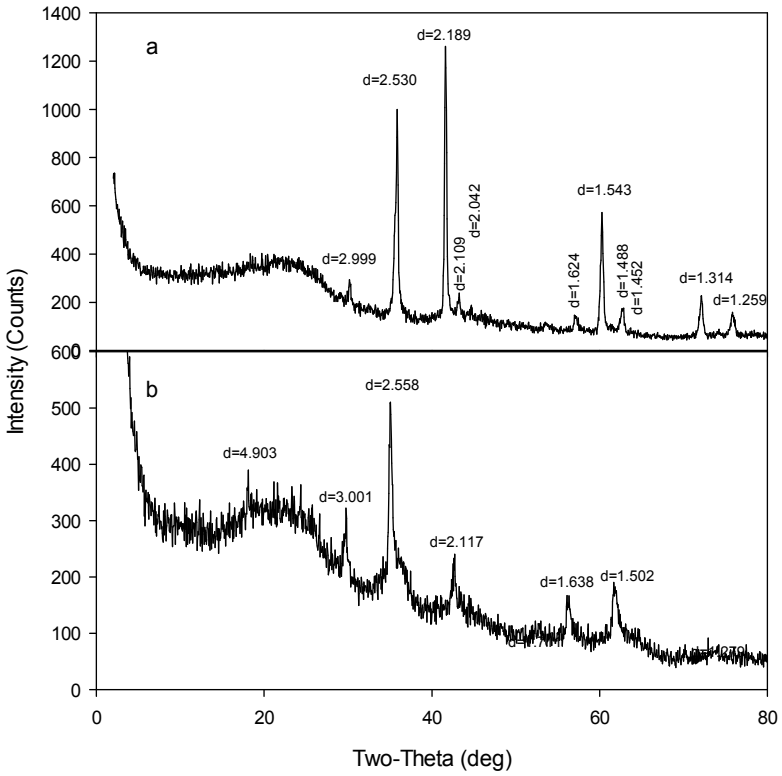

Figure 2. XRD diffraction patterns of FMM (a) and FMB (b)

Surface properties [32, 33] is important properties which may affect chemical and physical interactions on biochars surfaces. Compared to that of PB, the BET surface area was slightly higher in FMM, but lower in FMB (Table 1). The decrease in surface area of FMB was possibly due to relatively low surface area of bimetal oxides [34] or the co-precipitation process, which blocked the pores of the biochar.

The thermal stability of biochars was evaluated using thermogravimetric analysis (TGA) by combustion between 25 and 700 ^{o}C under air atmosphere (Figure 3). TGA curves are comprised of three stages, with a stable phase up to 300-400 ^{o}C followed by a rapid weight loss phase up to 500 -530 ^{o}C, and finally a stable phase until 700 ^{o}C. The turning point between the first and second phases is an indication of the thermal stability of biochars, showing that PB and FMB were more thermally stable than FMM. The rapid weight loss in the second phase could be

attributed to the combustion of carbonaceous materials in PB, and transformation of non-volatile elements such as Mn oxides in FMM and FMB [5, 35]. Decreased thermal stability of FMM may be related to the appearance of Mn oxides. Ash content of PB increased from 4.0% to 18.1% in FMM and 31.9% in FMB, indicating metals, which would not be volatilized, were introduced in the synthetic process. Higher ash content of FMB than FMM suggests that more Mn and Fe were introduced during the co-precipitation, which is consistent with the elemental analysis data.

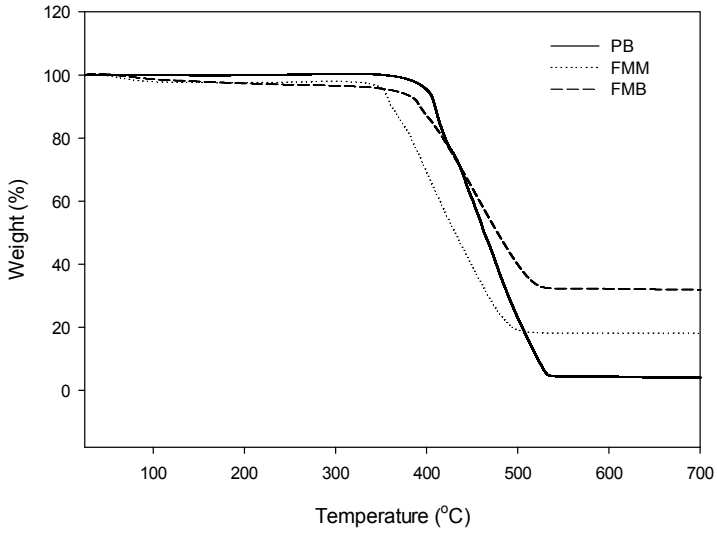

Figure 3. TGA curves of PB, FMM and FMB

3.2 *As(V) sorption kinetics*

Batch sorption experiment was conducted to investigate the As(V) sorption kinetics of the two biochar composites and the pristine biochar. The kinetics of three biochars exhibited a

Table 2. Kinetics models and best-fit parameters of As(V) sorption onto biochars.

Model/Equations	Biochar	Parameter1	Parameter2	R^2
First-order	PB	q_e=0.128 g kg^{-1}	k_1=1.66 h^{-1}	0.814
$q_t = q_e(1-e^{-k_1 t})$	FMM	q_e=0.323 g kg^{-1}	k_1=0.762 h^{-1}	0.899
	FMB	q_e=2.45 g kg^{-1}	k_1=0.451 h^{-1}	0.964

Second-order	PB	q_e=0.139 g kg^{-1}	k_2=16.15 kg g^{-1} h^{-1}	0.900
$q_t = k_2 q_e^2 t / (1 + k q_e t)$	FMM	q_e=0.356 g kg^{-1}	k_2=2.67 kg g^{-1} h^{-1}	0.951
	FMB	q_e=2.67 g kg^{-1}	k_2=0.239 kg g^{-1} h^{-1}	0.986
Elovich	PB	α= 7.86 g kg^{-1}	β=66.45 g kg^{-1}	0.961
$q_t = \beta^{-1} \ln(\beta \alpha t + 1)$	FMM	α=1.41 g kg^{-1}	β=18.27 g kg^{-1}	0.975
	FMB	α= 5.99 g kg^{-1}	β=2.30 g kg-1	0.963

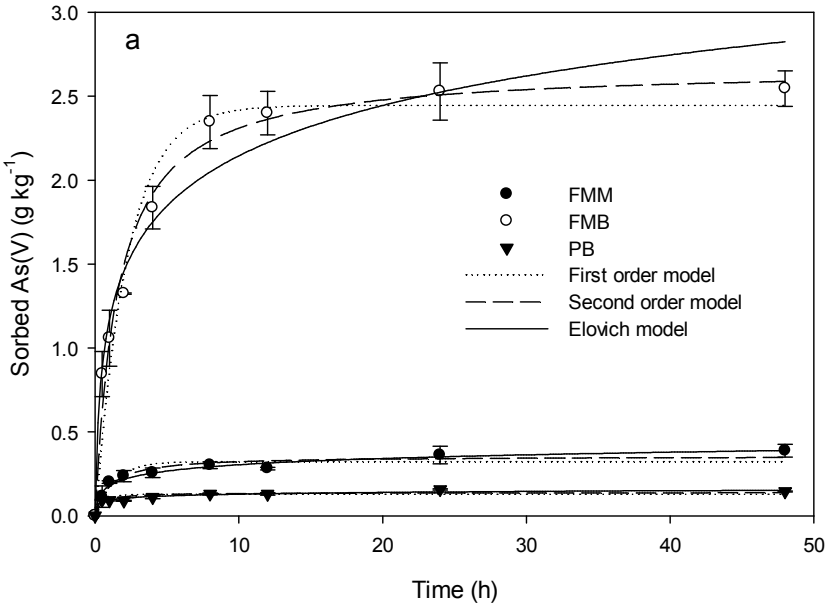

Figure 4 As(V) sorption kinetics and fitted models. Sorbent 2.5g L^{-1}, pH 7.5

rapid sorption phase (Figure 4), which was achieved within 8 h, followed by a slow sorption phase until equilibrium. The sorption kinetics data were fitted with pseudo-first-order, pseudo-second order, and Elovich kinetic models. The second order and Elovich models are better fitted models with R^2 above 0.95 (Table 2). Based on the fitted Elovich model, the FMB has higher initial adsorption rate (α) of As(V) than FMM while FMM has higher desorption potential (β) than FMB. PB has the highest β value, suggesting that modified biochars have greater affinity for

As(V) in aqueous solution. Good fit of second and Elovich models implies that As(V) was retained with several possible mechanisms.

3.3 *As(V) sorption isotherms*

Table 3. Isotherm models and best-fit parameters of As(V) sorption onto sorbents.

Model/Equations	Biochar	Parameter1	Parameter2	R^2
Langmuir	PB	S_{max}= 0.200 g kg^{-1}	K=0.316 L g^{-1}	0.991
$S = S_{max} KC / (1 + KC)$	FMM	S_{max}=0.500 g kg^{-1}	K=0.491 L g^{-1}	0.985
	FMB	S_{max}=3.44 g kg^{-1}	K=0.377 L g^{-1}	0.991
Freundlich	PB	n=0.332	K_f=0.068 $g^{(1-n)}$ L^n kg^{-1}	0.995
$S = K_f C^n$	FMM	n=0.342	K_f=0.181 $g^{(1-n)}$ L^n kg^{-1}	0.981
	FMB	n=0.504	K_f=0.893 $g^{(1-n)}$ L^n kg^{-1}	0.972

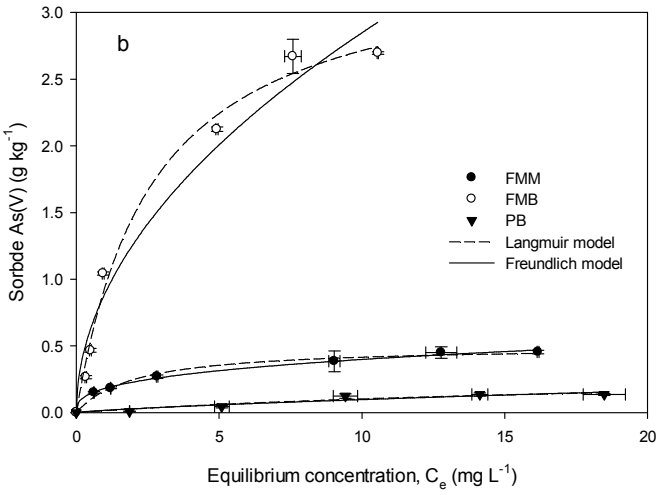

Figure 5. Sorption isotherms of As(V) sorption onto biochars. Sorbent 2.5g L^{-1}, pH 7.5

Sorption isotherms are generally used to estimate the maximum sorption potential of adsorbents. Although the optimal As(V) sorption pH was later found to be at 3 within the tested pH range, the isotherm in this study was conducted at pH 7.5 to determine the maximal sorption capacity at around neutral pH.

Sorption isotherms were all L-shaped (Figure 5) and fitted well with both Langmuir and Freundlich models ($R^2 > 0.97$) (Table 3). The Langmuir maximum sorption capacities (S_{max}) of

FMM and FMB were about 2.5 and 17 times greater than that of PB, respectively, suggesting the bimetal modification can improve As(V) onto biochar. The results also indicate that co-precipitation of $MnFe_2O_4$ on biochar is a more effective approach to prepare Fe-Mn biochar composites for As(V) removal than the pyrolysis method.

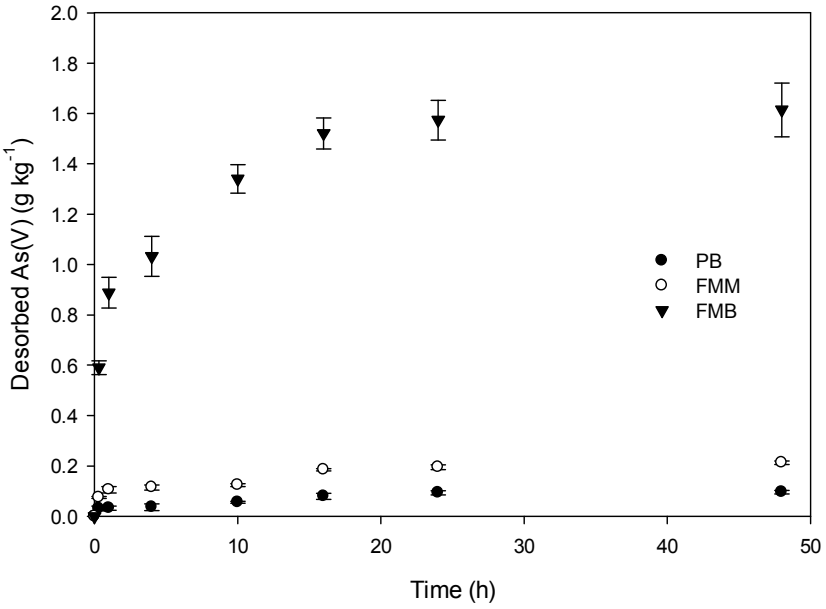

Figure 6. Desorption of As(V) with time from PB, FMM and FMB. Initial As(V)=20 mg L^{-1}. Sorbent 2.5g L^{-1}, pH=7.5.

3.4 *As(V) desorption study*

Desorption potential is an important characteristic that evaluates the regeneration of a sorbent. In the 0.1 M NaOH solution, most sorbed As(V) was desorbed within 10-15 h for all three sorbents (Figure 6), indicating that As(V) can be easily desorbed by NaOH for adsorbent regeneration. After desorption, 60.0 % and 46.7 % of sorbed As(V) was desorbed by 0.1 M NaOH in As loaded FMB and FMM, respectively. This is consistent with findings of studies that use sodium bicarbonate ($NaHCO_3$) and sodium hydroxide (NaOH) to desorb As(V) from carbon sorbents. For example, 0.05 $NaHCO_3$ was able to desorb 85% of As(V) sorbed onto the Fe-

impregnated within 1h desorption process [36]. 99% of As(V) sorbed onto the $MnFe_2O_4$ and $MnFe_2O_4$-graphene oxide hybrid was released into the 1 M NaOH desorption solution [19].

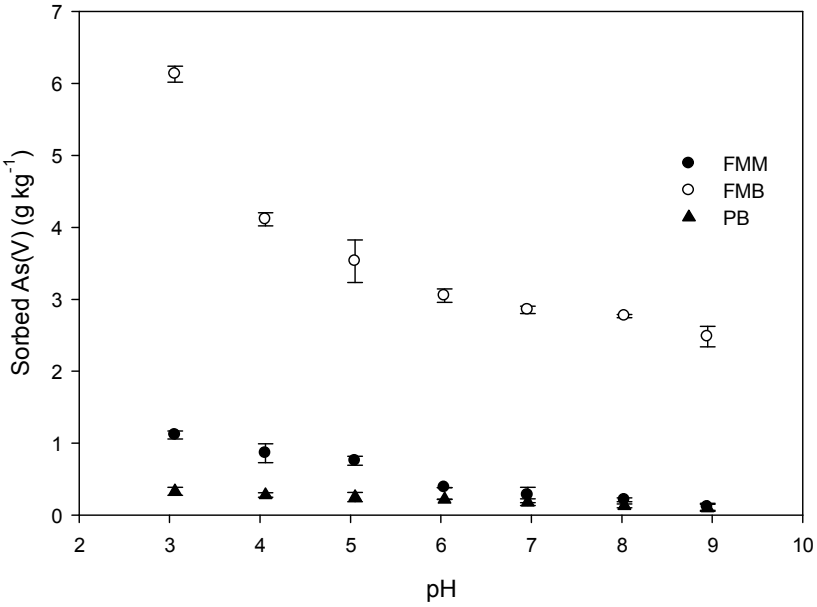

Figure 7. Effect of pH on As(V) sorption by biochars. Initial As(V)=40 mg L^{-1}. Sorbent 2.5g L^{-1}.

3.5 *pH effects on* As(V) *sorption*

The experimental results showed that between the pH values of 3 and 9, As sorption by FMM and FMB decreased with increasing pH (Figure 7). The As(V) sorbed at pH 9 decreased by 2.5 and 10 times than hat at pH 3 for FMB and FMM, respectively. This finding agrees with previous study on changes in As(V) sorption with varying pH [19].

pH affects surface charges by protonation and deprotonation of surface groups such as hydroxyl (-OH) group. As(V) exist predominately as $H_2AsO_4^-$ below pH 6.9 and $HAsO_4^{2-}$ between pH 6.9 and 11.5 (Figure 8) [26]. At lower pH, -OH tends to protonates and attracts negatively charged oxyanions, and thus increased As sorption.

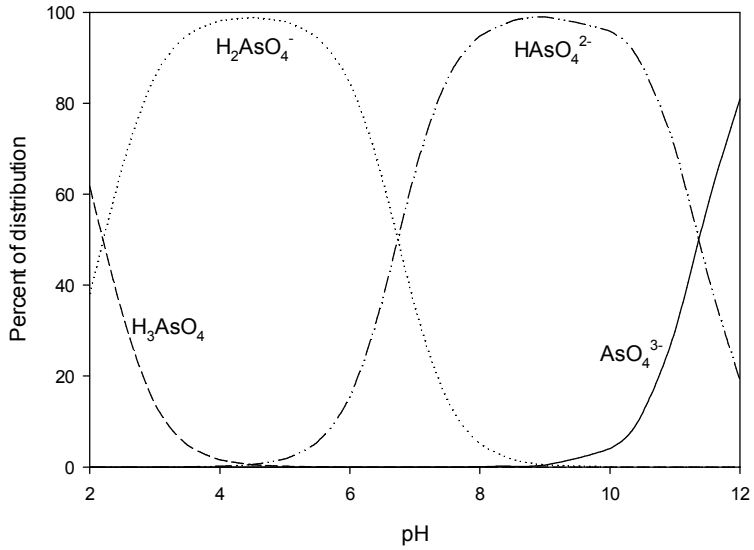

Figure 8. As(V) species distribution diagram between pH 2-12. Initial As(V)=0.53 mM, I=0.05M

3.6 As(V) *sorption mechanisms*

As(V) sorption capacity of pristine biochar is low (0.200 g kg^{-1}), and thus the increased sorption for FMM and FMB should attribute to the presence of the dual metal oxides (MnO and γ-Fe_2O_3) and the bimetal oxides ($MnFe_2O_4$), respectively. FMM showed much lower As(V) sorption capacity than that of many other metal oxide biochar composites [11, 12, 14], suggesting that presence of additional Mn oxides within the biochar may not guarantee the enhanced sorption of As(V) in aqueous solution. The As(V) sorption capacity of FMB was much higher than that of the FMM. This can be attributed to the formation of bimetal oxides on the C surfaces of biochars. Previous studies have shown that the As(V) sorption capacity of the $MnFe_2O_4$ [4, 19] is much larger than that of MnO [37, 38] or γ-Fe_2O_3 [39, 40].

Multiple mechanisms may participate in the As(V) sorption by the sorbents. The higher surface area but lower As(V) sorption capacity in FMM indicate surface area is not an important

factor controlling As sorption, suggesting physico-sorption is not a governing mechanism for As(V) sorption.

Other possible mechanisms are proposed. On one hand, the positively charged surfaces of FMM and FMB may attract the negatively charged As oxyanionic species. At experimental pH of 7.5, As(V) mainly exists as negatively charged anions, such as $HAsO_4^{2-}$ (85.4%) and $H_2AsO_4^-$ (14.6%) (Figure 8) with negative zeta potential [20]. In aqueous solutions, surfaces of dual metal oxides and Mn ferrite in FMM and FMB can be hydroxylated, and thus have pH dependent surface charges, generated by the deprotonation and protonation of hydroxyl (-OH) group [28]. Previous studies showed that maghemite has pHpzc greater than 8.4 [41], and the pHpzc of jacobite as well as some other ferrite bimetal oxides such as cobalt and nickel ferrite is around or above 8 [41, 42]. Thus, the pHpzc of both FMM and FMB should probably possess pHpzc greater than 7.5. Thus, both FMM and FMB are positively charged and attract $H_2AsO_4^-$ and $HAsO_4^{2-}$ by electrostatic attractions. Lower pH can promote the protonation of the bimetal or metal oxides to introduce more positive surface charges [28, 43]. As a result, it will increase the attractive electrostatic forces to enhance the sorption of As(V) onto the biochar composites. In contrast to lower pH, the surfaces of the bimetal or metal oxides will be dominantly negatively charged which reduced the As(V) sorption when solution pH increases, particularly to above pHpzc, Hydroxylated $MnFe_2O_4$ surfaces can electrostatically attract negatively charged As(V) to form complexes [19, 20, 44], such as:

$$S_{Mn-Fe}-OH_2^+ + H_2AsO_4^- \Leftrightarrow S_{Mn-Fe}-OH-H_3AsO_4 \quad (1) \quad (\text{pH} < 6.9)$$

or $$2S_{Mn-Fe}-OH_2^+ + HAsO_4^{2-} \Leftrightarrow (2S_{Mn-Fe}-OH)-H_3AsO_4 \quad (2) \quad (6.9 < \text{pH} < 7.5)$$

where $S_{Mn\text{-}Fe}$ denotes the $MnFe_2O_4$ surface.

On the other hand, isotherm and kinetics models implied that other mechanisms may act in addition to electrostatic attraction. XPS analysis was used to identify the interaction between biochar composites and As(V). O1s peaks of both FMM and FMB were divided into two peaks at binding energy, namely, 530.33-530.58 eV and 532.80-532.85 eV (Figure 9). After As(V) sorption, three O1s peaks were deconvoluted into three peaks at 530.23-530.33 eV, 531.41-531.70 eV, and 533.13-533.55 eV (Figure 9), which can be assigned to O bonded to metal, and hydroxyl (-OH) bonded to metal, and –OH bonded to C [20, 45, 46]. These results confirm the mechanism that aqueous As(V) can complex with –OH to form M-O-As bond in both FMM and FMB [20, 47].

To conclude, As(V) sorption by both FMM and FMB occurs by electrostatic attraction and surface complexation.

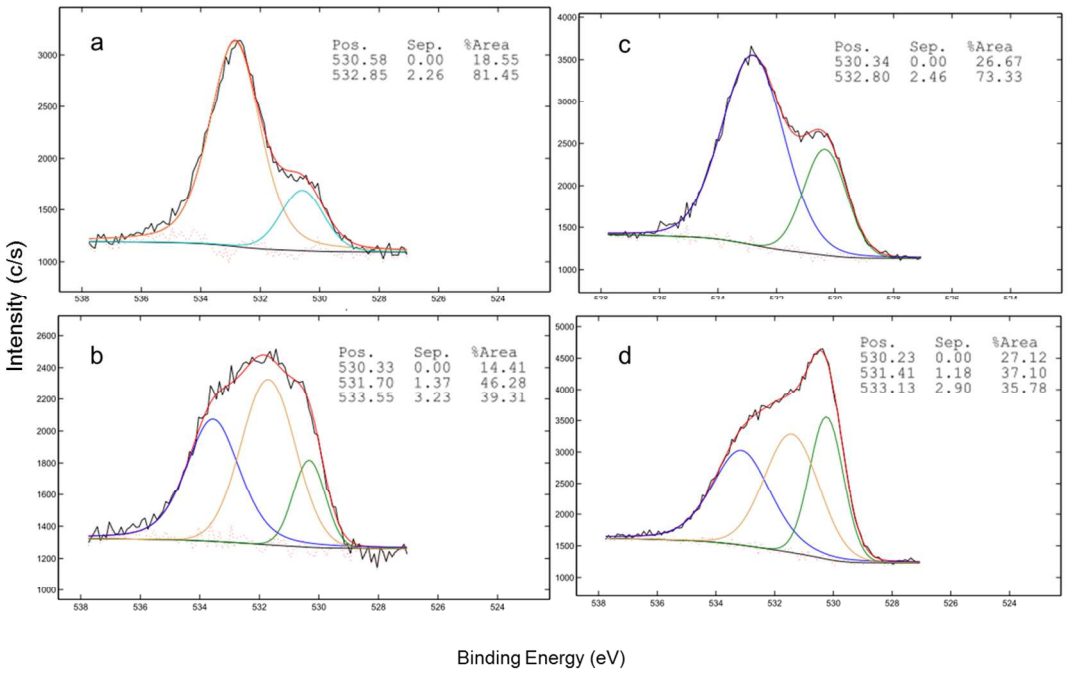

Figure 9. O1s peaks of FMM (a), As(V)-laden FMM (b), FMB (c), and As(V)-laden FMB (d).

4. Conclusions

Co-precipitation method produces bimetal oxides, $MnFe_2O_4$, on biochar surfaces, which showed better As(V) sorption ability than the biochar composites with dual metal oxides prepared from pyrolysis. The sorption of As(V) on the two magnetic Fe-Mn biochar composites was pH dependent. In addition, 0.1 M NaOH solution released the adsorbed As(V) from the adsorbents. Findings from this work suggest that the enhanced sorption of As(V) onto the magnetic biochar composites is mainly through electrostatic attractions of As(V) by positive surface charges and surface complexation with surface groups of the bimetal or metal oxides on the C surfaces.

Acknowledgments

This research was partially supported by the NSF through grants: CBET-1054405 and CHE-1213333.

References

1. S. K. Singh, A. K. Ghosh, A. Kumar, K. Kislay, C. Kumar, R. R. Tiwari, R. Parwez, N. Kumar and M. D. Imam, *International Journal of Environmental Research*, 2014, **8**, 49-60.

2. Y. Zhang, M. Yang, X.-M. Dou, H. He and D.-S. Wang, *Environ Sci Technol*, 2005, **39**, 7246-7253.

3. U.S.EPA, *Journal*, 2000, **EPA 815-R-00-028**.

4. S. Zhang, H. Niu, Y. Cai, X. Zhao and Y. Shi, *Chem Eng J*, 2010, **158**, 599-607.

5. S. Wang, B. Gao, Y. Li, A. Mosa, A. R. Zimmerman, L. Q. Ma, W. G. Harris and K. W. Migliaccio, *Bioresource Technol*, 2015, **181**, 13-17.

6. Y. Yao, B. Gao, M. Inyang, A. R. Zimmerman, X. Cao, P. Pullammanappallil and L. Yang, *Bioresource Technol*, 2011, **102**, 6273-6278.

7. B. K. Mandal and K. T. Suzuki, *Talanta*, 2002, **58**, 201-235.

8. J. F. Ferguson and J. Gavis, *Water Res*, 1972, **6**, 1259-1274.

9. B. Lafferty, M. Ginder-Vogel and D. Sparks, *Environ Sci Technol*, 2010, **44**, 8460-8466.

10. J. Gimenez, M. Martinez, J. de Pablo, M. Rovira and L. Duro, *J Hazard Mater*, 2007, **141**, 575-580.

11. M. Zhang and B. Gao, *Chem Eng J*, 2013, **226**, 286-292.

12. M. Zhang, B. Gao, S. Varnoosfaderani, A. Hebard, Y. Yao and M. Inyang, *Bioresource Technol*, 2013, **130**, 457-462.

13. Y. Yao, B. Gao, J. Chen, M. Zhang, M. Inyang, Y. Li, A. Alva and L. Yang, *Bioresource Technol*, 2013, **138**, 8-13.

14. S. Wang, B. Gao, A. Zimmerman, Y. Li, L. Ma, W. Harris and K. Migliaccio, *Bioresource Technol*, 2015, **175**, 391-395.

15. M. G. Naseri, E. B. Saion and A. Kamali, *ISRN Nanotechnology*, 2012, **2012**.

16. A. Elfalaky and S. Soliman, *J Alloy Compd*, 2013, **580**, 401-406.

17. B. Bateer, C. Tian, Y. Qu, S. Du, Y. Yang, Z. Ren, K. Pan and H. Fu, *Dalton Transactions*, 2014, **43**, 9885-9891.

18. Y. Xiao, J. Zai, L. Tao, B. Li, Q. Han, C. Yu and X. Qian, *Phys Chem Chem Phys*, 2013, **15**, 3939-3945.

19. S. Kumar, R. R. Nair, P. B. Pillai, S. N. Gupta, M. A. R. Iyengar and A. K. Sood, *ACS Appl Mater Interfaces*, 2014, DOI: 10.1021/am504826q.

20. W. Tang, Y. Su, Q. Li, S. Gao and J. K. Shang, *Water Res*, 2013, **47**, 3624-3634.

21. Y.-J. Tu, C.-F. You, C.-K. Chang, S.-L. Wang and T.-S. Chan, *Chem Eng J*, 2012, **198–199**, 440-448.

22. S. C. Peterson, M. Appell, M. A. Jackson and A. A. Boateng, *Journal of Agricultural Science (Toronto)*, 2013, **5**, 1-8.

23. K. Hammes, R. J. Smernik, J. O. Skjemstad and M. W. I. Schmidt, *Appl Geochem*, 2008, **23**, 2113-2122.

24. S. Goldberg and C. Johnston, *J Colloid Interf Sci*, 2001, **234**, 204-216.

25. G. J. Liu, X. R. Zhang, L. McWilliams, J. W. Talley and C. R. Neal, *Journal of Environmental Science and Health, Part A*, 2008, **43**, 430-436.

26. Y. Mamindy-Pajany, C. Hurel, N. Marmier and M. Roméo, *Comptes Rendus Chimie*, 2009, **12**, 876-881.

27. J. Antelo, M. Avena, S. Fiol, R. López and F. Arce, *J Colloid Interf Sci*, 2005, **285**, 476-486.

28. Y. Yao, B. Gao, M. Inyang, A. R. Zimmerman, X. D. Cao, P. Pullammanappallil and L. Y. Yang, *J Hazard Mater*, 2011, **190**, 501-507.

29. S. Sarkar, L. M. Blaney, A. Gupta, D. Ghosh and A. K. SenGupta, *Environ Sci Technol*, 2008, **42**, 4268-4273.

30. X. Dong, L. Q. Ma and Y. Li, *J Hazard Mater*, 2011, **190**, 909-915.

31. L. Cabrera, Á. Somoza, J. Marco, C. Serna and M. Puerto Morales, *J Nanopart Res*, 2012, **14**, 1-14.

32. X. Li and Z. Li, *Journal of Chemical & Engineering Data*, 2010, **55**, 5729-5732.

33. X. Li, X. Chen and Z. Li, *Journal of Chemical & Engineering Data*, 2010, **55**, 3164-3169.

34. L. X. Yang, F. Wang, Y. F. Meng, Q. H. Tang and Z. Q. Liu, *J Nanom*, 2013, DOI: Artn 293464

Doi 10.1155/2013/293464.

35. C. Gonzalez, J. I. Gutierrez, J. R. GonzalezVelasco, A. Cid, A. Arranz and J. F. Arranz, *Journal of Thermal Analysis*, 1996, **47**, 93-102.

36. X. Hu, Z. Ding, A. R. Zimmerman, S. Wang and B. Gao, *Water Res*, 2015, **68**, 206-216.

37. S. Wang, B. Gao, Y. Li, A. Mosa, A. R. Zimmerman, L. Q. Ma, W. G. Harris and K. W. Migliaccio, *Bioresour Technol*, 2015, **181**, 13-17.

38. Q. Li, X. Xu, H. Cui, J. Pang, Z. Wei, Z. Sun and J. Zhai, *J Environ Manage*, 2012, **98**, 98-106.

39. S. R. Chowdhury, E. K. Yanful and A. R. Pratt, *Environ Earth Sci*, 2011, **64**, 411-423.

40. M. Auffan, J. Rose, O. Proux, D. Borschneck, A. Masion, P. Chaurand, J. L. Hazemann, C. Chaneac, J. P. Jolivet, M. R. Wiesner, A. Van Geen and J. Y. Bottero, *Langmuir*, 2008, **24**, 3215-3222.

41. M. Kosmulski, *J Colloid Interf Sci*, 2009, **337**, 439-448.

42. F. Tourinho, R. Franck and R. Massart, *J Mater Sci*, 1990, **25**, 3249-3254.

43. P. W. Schindler and W. Stumm, in *Aquatic surface chemistry - chemical processes at the particle-water interface.*, ed. W. Stumm, John Wiley & Sons, New York, 1987.

44. K.-H. Goh, T.-T. Lim and Z. Dong, *Environ Sci Technol*, 2009, **43**, 2537-2543.

45. S. Deng and Y. P. Ting, *Environ Sci Technol*, 2005, **39**, 8490-8496.

46. J. L. Wan, H. P. Deng, J. Shi, L. Zhou and T. Su, *Clean-Soil Air Water*, 2014, **42**, 1199-1207.

47. M. J. Eick, J. D. Peak and W. D. Brady, *Soil Sci Soc Am J*, 1999, **63**, 1133-1141.

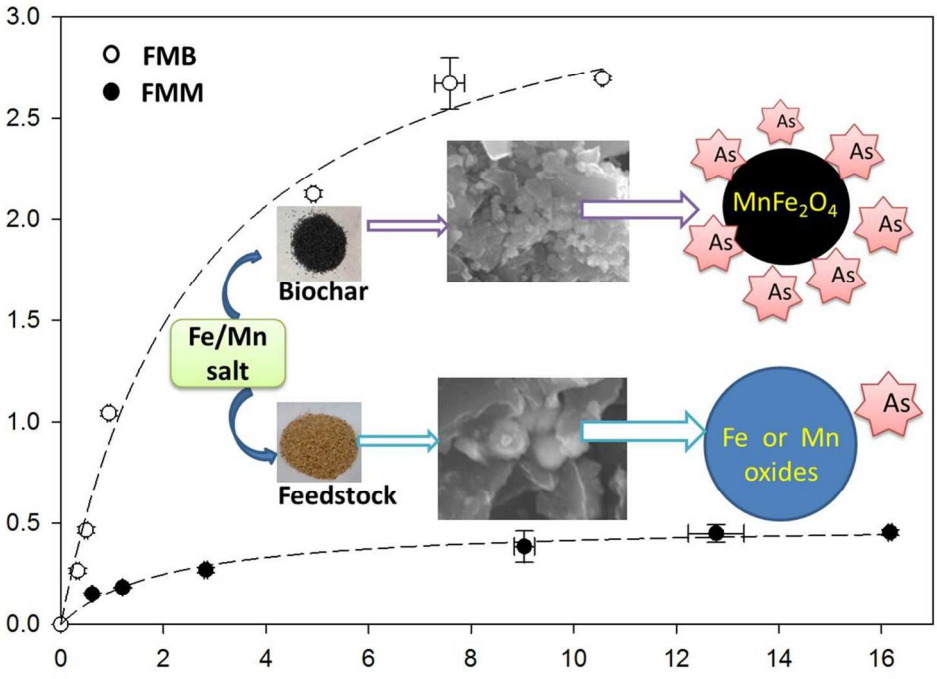

221x161mm (150 x 150 DPI)